Structural Characterization of Human RPA Sequential Binding to Single-Stranded DNA Using ssDNA as a Molecular Ruler †

ARTICLE *in* BIOCHEMISTRY · AUGUST 2007

Impact Factor: 3.02 · DOI: 10.1021/bi7004976 · Source: PubMed

6 AUTHORS, INCLUDING:

Lifeng Cai
Academy of Military Medical Sciences
42 PUBLICATIONS **490** CITATIONS
SEE PROFILE

Marina Roginskaya
East Tennessee State University
18 PUBLICATIONS **255** CITATIONS
SEE PROFILE

Yue Zou
East Tennessee State University
67 PUBLICATIONS **2,072** CITATIONS
SEE PROFILE

Published in final edited form as:
Biochemistry. 2007 July 17; 46(28): 8226–8233. doi:10.1021/bi7004976.

A Structural Characterization of Human RPA Sequential Binding to Single-Stranded DNA Using ssDNA as a Molecular Ruler

Lifeng Cai[‡], **Marina Roginskaya**[‡], **Youxing Qu**[$], **Zhengguan Yang**[‡], **Ying Xu**[$], and **Yue Zou**[‡,*]

‡ *Department of Biochemistry and Molecular Biology, James H. Quillen College of Medicine, East Tennessee State University, Johnson City, Tennessee 37614*

$ *Department of Biochemistry and Molecular Biology, University of Georgia, Athens, GA 30602-7229 and Computational Biology Institute, Protein Informatics Group, Life Sciences Division, Oak Ridge National Laboratory, Oak Ridge, TN 37830, USA*

Abstract

Human replication protein A (RPA), a heterotrimer composed of RPA70, RPA32, and RPA14 subunits, contains four single-stranded DNA (ssDNA) binding domains (DBD): DBD-A, DBD-B and DBD-C in RPA70 and DBD-D in RPA32. While crystallographic or NMR structures of these DBDs and a trimerization core have been determined, the structure of the full length of RPA or RPA-ssDNA complex remains unknown. In this report, we have examined the structural features of RPA interaction with ssDNA by fluorescence spectroscopy. Using a set of oligonucleotides (dT) with varying lengths as a molecular ruler and also as the substrates, we have determined at single nucleotide resolution the relative positions of the ssDNA-interacting intrinsic tryptophans of RPA. Our results revealed that Trp528 in DBD-C and Trp107 in DBD-D contact ssDNA at the 16th and 24th nucleotides (nt) from the 5′-end of the substrate, respectively. Evaluation of the relative spatial arrangement of RPA domains in RPA-ssDNA complex suggested that DBD-B and DBD-C are spaced by about 4 nt (~19 Å) apart while DBD-C and DBD-D by about 7 nt (~34 Å). Based on these geometric constraints, a global structure model for the binding of the major RPA DBDs to ssDNA was proposed.

Keywords

Replication protein A; single-stranded DNA; RPA-ssDNA binding; structural characterization; and fluorescence spectroscopy

INTRODUCTION

Replication protein A (RPA)[1] is a eukaryotic single-stranded DNA (ssDNA) binding protein. The hallmark ssDNA binding activity of RPA is essential for its functions in DNA replication, repair and recombination (1–7), as well as in ATR and Rad9/Rad1/Hus1-mediated DNA damage responses (8–10). In cells, RPA binds tightly to the ssDNA regions generated during these DNA metabolic reactions, and interacts with many other proteins to facilitate these

*To whom correspondences should be addressed: Yue Zou, East Tennessee State University, James H. Quillen College of Medicine, Department of Biochemistry and Molecular Biology, Johnson City, TN 37614, Phone: (423) 439-2124, FAX: (423) 439-2030, email: zouy@etsu.edu.

[1]Abbreviation: RPA, replication protein A; ssDNA, single stranded DNA; dsDNA, double stranded DNA; DBD, DNA binding domain; OB, oligonucleotide/oligosaccharide binding; nt, nucleotide; ATR, ataxia-telangiectasia mutated- and Rad3-related.

processes. RPA also undergoes hyperphosphorylation in response to a variety of DNA damage agents such as UV or ionizing irradiation. The hyperphosphorylation is believed to play an important role in regulating RPA activities in cells (1,3,11–19). Structurally, human RPA is a heterotrimeric protein composed of three subunits of 70, 32 and 14 kDa (7), referred to as RPA70, RPA32 and RPA14, respectively.

Human RPA binds to ssDNA with low cooperativity and high affinity with an association constant (K_a) in the range of 10^8 to 10^{11} M^{-1} depending on the sequence and length of the substrate, and the experimental conditions (2,20–22). RPA contains four major DNA binding domains (DBDs). Three of them (DBD-A, -B and -C) are located in RPA70 in tandem, with DBD-A and -B in the central region and DBD-C in the C-terminal region (23). The fourth DBD resides in the central region of RPA32, referred to DBD-D (24,25). RPA binds to ssDNA in a sequential multi-step manner and in the direction from 5′ to 3′ (4,7,24–30). The binding is initiated by an interaction of the DBD-AB domains with a length of 8–10 nucleotides (nt) at 5′-terminus of the ssDNA (24). A more stable intermediate binding mode of 13 – 22 nt has been suggested with the additional involvement of DBD-C (4,24,25). Finally, the cooperative binding of all four RPA DBDs occurs with an occluded size of approximately 30 nt (4,7,31). It has been suggested that the involvement of DBD-C and DBD-D in the binding requires significant changes to the RPA conformation (4,25), while the conformation of ssDNA in the binding remains unknown. The binding of RPA to ssDNA of different lengths is always stoichiometric so that the binding stoichiometry is independent of the length of ssDNA (21, 31).

Important information of RPA domain structures has been obtained from X-ray crystallographic and NMR spectroscopic characterizations. This includes DBD-A and -B in the presence and absence of ssDNA (32–36), DBD-DRPA14 dimer (37), DBD-C/DBD-D/RPA14 trimer (24), the C-terminal domain of RPA32 (38) and the N-terminal domain of RPA70 (35,39). While almost all of the substructures of RPA have been solved, the global structure of the full length of intact RPA and the structure of the RPA-ssDNA complex remain unknown. The three-dimensional positioning of the RPA subunits becomes even more important as RPA may undergo structural changes and domain reorganization upon binding to ssDNA (40) (30–32,41,42). Furthermore, since RPA contains six OB (oligonucleotide/oligosaccharide-binding) folds, it remains to be determined whether other OB folds (RPA14 and the N-terminal domain of RPA70) also are involved in ssDNA interactions (30,43). We recently identified several lysines of full length of RPA directly involved in the interaction with ssDNA using a mass spectrometry-based method (44). However, more detailed structures of RPA in the complex, particularly the domain organization, remain to be defined. Availability of structural information on the intact RPA-ssDNA interactions is crucial for understanding the molecular mechanism of RPA and its biological functions.

In this report, using ssDNA as a molecular ruler and also as substrate, we have investigated structural features of the sequential binding of RPA to ssDNA by fluorescence spectroscopy. Our results showed that the intrinsic tryptophan fluorescence of RPA was quenchable upon binding to ssDNA due to the interactions between nucleotides and the tryptophan residues at the binding sites. Interaction of RPA with an array of increasing lengths of oligonucleotides $(dT)_n$ resulted in a “stair-like” pattern of fluorescence quenching as a function of the length of oligonucleotides. Combined with the available domain structure data of RPA, our results indicated that the two tryptophans in the DNA-binding clefts of DBD-C and DBD-D contacted nucleotides 16 and 24 of ssDNA numbered from the 5′-end, respectively. As a result, the ssDNA-bound RPA may adopt a structure with inter-domain distances of about 4 nt and 7 nt between DBD-B and DBD-C and between DBD-C and DBD-D, respectively. The determined relative positioning information was then used as the spatial constraints in a structural modeling of RPA DBDs-ssDNA binding.

MATERIALS AND METHODS

Materials

RPA protein was purified as described previously (45). Oligonucleotides of different lengths were purchase from MWG Genetic, acrylamide (40%) was from Bio-Rad, and *Escherichia coli* strain BL-21(DE3)-RP was from Stratagene. All other reagents are of molecular biology grade quality or better.

Buffer

RPA binding buffer contains 40 mM HEPES-KOH, pH 7.8, 75 mM KCl, 8 mM $MgCl_2$, 1 mM DTT, 10% glycerol, and 100 μg/mL BSA. RPA storage buffer consists of 30 mM HEPES-KOH, 0.25 mM EDTA, 0.01% NP-40, 1 mM DTT, 100 mM NaCl, 50% glycerol, pH 7.8.

Site-specific mutations of RPA

The double mutations of W528F (RPA70) and W107F (RPA32) were made in RPA with the pTYB-RPA plasmid as a template using the Stratagene QuikChang® MutiSite-Directed Mutagenesis Kit, by following the manufacturer's instruction. The cDNA of the RPA mutant coded in the constructed plasmid was overexpressed and the produced protein mutant was purified as described previously (45). The similar procedures were employed to construct the plasmid for overexpression of RPA mutant W528A and to purify the mutant protein.

Gel mobility shift assays

5′-^{32}P-$(dT)_{30}$ ssDNA (4 nM) was incubated with varying concentrations of RPA protein at room temperature for 15 minutes in 20 μL of RPA binding buffer. After incubation, 2 μL of 80% (v/v) glycerol was added, and the mixtures were immediately loaded onto a 3.5% native polyacrylamide gel in TBE running buffer and electrophoresed at room temperature.

Fluorescence measurements

Fluorescence measurements were performed on a SPEX Fluorolog-3 fluorometer (Jobin Yvon Inc.) with slit widths set at 3 and 5 nm for excitation and emission beams respectively. All measurements were performed in a micro quartz cuvette (4×4 mm; 220 μl) with a 2×2 mm stirring bar, and the temperature was set at 25 °C. The temperature was controlled by a LFI-3751 Peltier temperature controller (Wavelength Electronics, Inc). All fluorescence intensities were corrected by subtracting the buffer blank under the same conditions.

For fluorescence determination of RPA binding to different lengths of oligonucleotide dT, RPA (90 nM) was incubated with $(dT)_n$ (2 μM) with the length as indicated. After incubation in 220 μ1 RPA binding buffer at 25 °C for 10 min the fluorescence was recorded from 320 through 380 nm with the excitation wavelength set at 295 nm. The fluorescence intensity of free RPA was defined as F_0, and the fluorescence intensity of RPA bound to ssDNA as F. The % quenching of RPA tryptophan fluorescence upon ssDNA binding was defined as $(F_0\text{-}F)/F_0\times 100\%$. No more than 5% photobleaching was observed under these conditions.

Structural modeling of RPA DBDs-ABCD-$(dT)_{26}$ ssDNA complexes

The modeling work was performed using InsightII software (Accelrys, CA) followed by energy minimization using xplor-NIH (46) at each step where a nucleotide was added or a complex was formed. The model was made to keep the DBDs-CD complex and the three helix trimerization core intact, while the ssDNA was bended at DBD-C, but remained straight between DBD-C and D domains.

Coordinates of DBDs-AB-8nt ssDNA complex were taken from PDB code 1jmc (33), DNA-free DBD-C, D domains and RPA14 protein were from PDB code 1110 (24). Based on the crystal structure of the 8 nucleotides (in a roughly straight form) bound to DBDs-AB, it was estimated that the average length of a nucleotide was approximately 4.8 Å. This distance constraint was applied throughout the modeling. Strong evidence suggested conserved DNA-binding site across all four DBD domains, with each DBD domain binding about three nucleotides in a very similar manner (33). Therefore, structures of DBD-C-3nt and DBD-D-3nt ssDNA complexes were modeled following the method of Bochkareva *et al.* (24) by aligning homologous structural elements. From the modeled DBD-C-3nt complex structure, it was observed that the last bound nucleotide in the 3nt ssDNA was not in close contact with W528. From this nucleotide, the ssDNA chain needs approximately one more nucleotide to get close enough to quench the fluorescence of W528. Our experiment data indicated the fluorescence of W528 was quenched by dT16. So the 3 nucleotides bound to DBD-C were deduced to be 13^{th} – 15^{th} nt, which was in good agreement with the work of others (40). For the DBD-D-3 nt complex, the first bound nucleotide of the 3nt ssDNA interacted directly with W107. In accordance with our fluorescence quenching data, the 3 nucleotides bound to DBD-D were determined to be dT24–26.

The flexible 18-residue loop between DBD-B and C was added in the modeling. The gap distance between dT8 and dT13 was set to 19 Å (4 nt), assuming the same straight ssDNA conformation as observed between DBD-A and B domains. The straight distance of the DNA gap between dT15 and dT24 was set to 38 Å (8 nt) which was found to fit quite nicely to the intact DBDs-CD protein complex structure.

RESULTS

Binding of RPA to ssDNA of increasing lengths

RPA contains eight tryptophan residues: W197 and W212 in DBD-A, W361 and W414 in DBD-B, and W442 and W528 in DBD-C of RPA70; W2 in the flexible N-terminal region of RPA32, and W107 in DBD-D of RPA32. Analysis of the available RPA domain structures (4,24,30,33) indicates that among these residues, W212, W361 and W528 of RPA70, and W107 of RPA32 reside in the ssDNA-binding clefts of DBD-A, B, C, and D, respectively, while the other Trp residues are located far away from the binding cleft structures (Figure 1). Co-crystal structure of DBDs-AB with an 8 nt ssDNA showed the direct involvement of W212 and W361 in binding (33). It is likely that tryptophans W528 and W107 also are involved in the ssDNA interactions, and such interaction may result in significant fluorescence changes of these residues upon ssDNA binding. To obtain the structural information on the sequential step-wise binding of RPA to ssDNA substrate, fluorescence of intrinsic tryptophans of RPA was recorded to monitor their interactions with single-stranded $(dT)_n$ substrates of increasing lengths. It should be pointed out that the binding of RPA to even the shortest ssDNA is believed to be stoichiometric (21,31). As shown in Figure 2A, in comparison with free RPA, tryptophan fluorescence of RPA was significantly reduced upon binding to $(dT)_8$ and $(dT)_{30}$ at saturating concentrations. It has been established that the RPA binding to $(dT)_8$ involved only the DBD-A and DBD-B domains, while binding to $(dT)_{30}$ required the participation of all four DNA-binding domains (4,24,30). The stronger quenching with $(dT)_{30}$ than $(dT)_8$ indicated the contributions to the quenching from tryptophans in DBD-C and DBD-D. Further investigation of RPA interaction with a series of different lengths of $(dT)_n$ demonstrated that the fluorescence quenching increased with the length (8 to 40 nt) of the substrates (Figure 2B, filled circles). But most strikingly, the relationship featured three plateaus and two sharply rising steps. Specifically, the extent of fluorescence quenching remained similar for RPA binding to the ssDNA of 8 – 15 nt, followed by a sharp and substantial increase of quenching for binding to $(dT)_{16}$. Considering that binding of RPA to ssDNA is a sequential process in the direction from

5′ to 3′ of ssDNA (4), this result suggests that the oligonucleotides $(dT)_{16}$, only one nt longer than $(dT)_{15}$, happened to be long enough to allow the 16th nucleotide at the 3′-end of substrate to interact with the W528 residue in DBD-C. The percentage of quenching remained unchanged again as the length of ssDNA for binding increased up to 23 nt. Then with one nt longer, interaction of RPA with $(dT)_{24}$ resulted in another significant increase in quenching, most likely induced by the interaction of the substrate with W107 in DBD-D of RPA32. Thereafter, the quenching started to increase gradually as the ssDNA was further lengthened, until reaching the maximum quenching (45%) for RPA binding to $(dT)_{30}$. No additional substantial change of fluorescence was observed for longer ssDNA (e.g. 40 nt) binding (Figure 2B, filled circles).

Binding of RPA mutants to ssDNA

To confirm that the "stair-like" fluorescence quenching was the direct results of the ssDNA interactions of W528 of DBD-C and W107 of DBD-D, the RPA protein with the double mutations of W528F/W107F was generated. The replacement of tryptophans with phenylalanine at residues 528 of DBD-C and 107 of DBD-D eliminated the Trp fluorescence contributions from these two sites, whereas the aromatic features of the residues which may be important for their ssDNA-interactions remained. Subsequent gel mobility shift assays indicated that this mutant protein was fully functional in ssDNA binding as compared with the native protein (Figure 3A). This was further confirmed by the fluorescence anisotropy determination of the RPA mutant interaction with $(dT)_{30}$ (Figure 3B). The dissociation constant for the binding is 0.8 ± 0.2 nM, which is equivalent to that for native RPA-$(dT)_{30}$ interaction (Table 1). The mutant protein was then subjected to Trp fluorescence measurements with the excitation wavelength set at 295 nm in the presence and absence of ssDNA. As shown in Figure 3C, similar to the case of native protein, binding of the RPA mutant to $(dT)_8$ resulted in a significant fluorescence quenching. However, unlike the case of native protein, interaction of the mutant protein with the $(dT)_{30}$ yielded the same extent of fluorescence reduction as with $(dT)_8$. In other words, no further fluorescence quenching was observed for the binding of $(dT)_{30}$ over that of $(dT)_8$, so that the "stair-like" quenching pattern was lost. These results strongly supportthat the W528 and W107 are responsible for the "stair-like" pattern of fluorescence quenching demonstrated in Figure 2.

To further verify the direct involvement of W528 in the interaction of RPA to ssDNA, the RPA mutant protein with the W528 residue substituted by an alanine (W528A) was purified. Then experiments were carried out to determine the fluorescence quenching of this mutant with varying length of ssDNA under saturation conditions. As shown in Figure 2B (open circles), the further quenching due to the binding of native RPA to $(dT)_{16}$ was no longer observed with RPA(W528A) mutant, strongly indicating that residue W528 is directly involved in the interaction with the 16th nt of $(dT)_{16}$ from the 5′-end. The fluorescence quenching remains essentially the same until the ssDNA longer enough to engage W107 of DBD-D. We also determined the binding affinity of RPA(W528A) mutant protein with $(dT)_{30}$. As listed in Table 1, the mutant binding is about 2-fold less efficient than that of native or wild-type RPA. The affinity loss is likely due to the absence of aromaticity or hydrophobicity at residue 528, again strongly suggesting a role of W528 in the RPA-ssDNA interaction.

Next we examined the binding of native RPA to a dT-30mer with an apyrimidinic (AP) site or without the base (dbase) at the 16th nucleotide from the 5′-end, referred as dT-30mer(AP16). The construction and use of this ssDNA substrate was to confirm the direct interaction of the 16th nt with residue W528. As shown in Figure 4, the lack of base at 16th nt caused a significant reduction in fluorescence quenching as compared with the binding with $(dT)_{30}$. This provided further evidence supporting the interaction of W528 with the 16th nt of the ssDNA.

A simple modeling of RPA DBDs-ssDNA interactions

Based on our fluorescence data, the structure of the interaction of RPA DBDs with a $(dT)_{26}$ ssDNA was modeled with the spatial constraints obtained above as described in the Experimental Procedures. As shown in Figure 5A, a structural model for the complex is produced with the assumption that the trimerization core has no significant conformational changes upon ssDNA binding, consistent with the previous report that there was essentially no change in the length of monomeric RPA upon binding to ssDNA (42). Based on the crystallographic structure of the core (24), the modeling results in only limited local structural alterations involving the DNA binding cleft residues. By contrast, the ssDNA was allowed to be bent along with the path of DNA binding cleft of DBD-C (Figure 5A). The fact that ssDNA is substantially flexible about its phosphodiester backbone makes it possible for the ssDNA to accommodate the major native structure of the core with appropriate bending. In the modeling, when the DBD-C-3 nt (dT13–15) complex and the DBD-D-3 nt (dT24–26) complex were first modeled, the straight distance between 3′-end of the 15th nt and 5′-end of the 24th nt which is around 38 Å (~8 nt), was found to be in a nice fit to our fluorescence-determined coordinates. Therefore, a straight 8-nt was reasonably inserted into the ssDNA chain between DBD-C and D domains. In addition, the model is consistent with the previous prediction that basic amino acids K488, K489, K588 were oriented in contact with the phosphate backbone of ssDNA (24), which also was confirmed by our experiments (44).

It is worth mentioning that the 18-amino acid loop linking the DBD-B and -C is likely very flexible due to the structurally disordered sequence. The loop structure shown in Figure 5A was only for the purpose to show that DBD-B and -C are linked together by this loop.

DISCUSSION

The present study used a combination of available structures (24,33) and spectroscopic analysis using ssDNA as a molecular ruler to orient the relative positions of the RPA subunits with respect to each other and ther ssDNA ligand. Results from our fluorescence spectroscopic studies showed that binding of ssDNA to RPA resulted in varying extents of tryptophan fluorescence quenching of the protein in a ssDNA-length dependent manner. Interestingly, the dependence of fluorescence quenching of RPA on the length of substrates (8 – 30 nt) was featured with a “stair-like” relationship (Figure 2). Our results in Table 1 and Figure 4 suggest that this pattern of fluorescence changes was likely due to the increasing involvement of more tryptophan residues in the binding. Consistently, the crystallographic structure of the complex of DBD-AB domains with a 8-nt ssDNA showed only limited structural alterations in the DNA binding clefts of the domains upon ssDNA binding (32,33). Furthermore all tryptophans in RPA are located either on the back of DBDs and the unstructured N-terminal region of RPA32 or in the DNA binding clefts (Figure 1). Despite these, the indirect effects on the tryptophans due to the possible conformational changes of RPA can not be completely excluded.

RPA binds to ssDNA with increasing length from 8 nt through 30 nt in a dynamic and sequential (5′ to 3′) manner (4,33). Since the affinity of RPA DBD domains for ssDNA follows the order: DBD-A, DBD-B > DBD-C > DBD-D, the binding starts with interaction of DBDs-AB with 8 nt (4,33). This partial complex formation produced the initial fluorescence quenching of tryptophan residues (Figure 2). The observation of two subsequent sharp increases of fluorescence quenching with $(dT)_{16}$ and $(dT)_{24}$ following a plateau, suggested that the ssDNA has to be at least 16 and 24 nt long to reach the specific tryptophans (W528 of DBD-C in RPA70, and W107 of DBD-D in RPA32) for direct contacts, respectively. In other words, the RPA-ssDNA complex may adopt a structure with the two tryptophans interacting with the 16th and 24th nucleotides (from the 5′-end) of ssDNA, respectively. In DBD-C, tryptophan W528 is located at the exit area of the inflexible palm of OB fold and the plane of its aromatic rings directly faces the path for ssDNA binding (Figure 1A) (24). This implies that W528 may

become engaged in the interaction with a nucleotide, causing quenching of the fluorescence, only when ssDNA is long enough (at least 16 nt) and protrudes through the OB fold of DBD-C. It is likely that any possible structure changes in the palm due to the binding of shorter ssDNA (8 to 15 nt) may have little effects on the fluorescence of W528 because it is located just outside the exit. On the other hand, binding of ssDNA longer than 16 nt should cause no further fluorescence change until next tryptophan is encountered as the additional nucleotides should be found in the hinge region between DBD-C and DBD-D. Therefore, a "stair-like" relationship of fluorescence quenching with the length of ssDNA resulted. It should be noted that a little different pattern of fluorescence quenching was observed for RPA binding to ssDNA substrates longer than 24 nt (Figure 2). This is because W107 in DBD-D is located in the flexible wing (or finger) and near the entrance area of ssDNA binding cleft (Figure 1A) (24). It has been suggested that this part (the wing) of domain may have a significant conformational change so as to wrap the ssDNA (33,37). This structural alteration may depend on the length of ssDNA ranged from 24 to 30 nt. Since W107 resides near the entrance site, the interaction of the 24^{th} nucleotide of $(dT)_{14}$ with W107 may cause a significant but not a full fluorescence quenching of this residue. When additional nucleotides (of ssDNA > 24 nt) are involved in the interactions with other residues in the same cleft, conformational change of the wing may facilitate and thus enhance the W107-nucleotide interaction, causing increase of the quenching. Alternatively, due to the much lower ssDNA affinity of DBD-D than other DBDs (2,4,33), it is also possible that the ssDNA shorter than 24 nt (e.g. 23 nt) may interact in close proximity with W107 with insufficient binding energy to associate significantly to it. Thus the unstable binding results in no substantial fluorescence change. However, when an additional nucleotide is added to the lengthening ssDNA (e.g. 24 nt), the binding is stoichiometric or stable sufficiently to induce the change in fluorescence at the tryptophan even if the additional nucleotide could associate to the next nt-binding site of the domain.

Kim *et al*. reported a similar fluorescence measurement using a much smaller number of oligonucleotide dTs of different lengths (27). The inconsistency between their results and ours is obviously due to their use of the excitation wavelength of 282 nm rather than the 295 nm we used. At 282 nm, both tyrosine and tryptophan were excited, and the recorded fluorescence emission was a combined signal of tryptophan and tyrosine (47). Furthermore, fluorescent resonance energy transfer might occur between these two types of residues when excited at 282 nm. Since RPA contains a total of 29 tyrosines, a great complexity in fluorescence signal was likely to result. Also importantly, more valuable interpretation of fluorescence data could not be made due to the lack of RPA domain structures at that time.

Based on our results and the known structures of the DBD domains of RPA and the complex structure of DBD-AB with 8-nt ssDNA, we have performed a modelng to predict the global structures of major DBDs ssDNA complex formation (Figure 5). The model represents a scenario in which the RPA binds to a bent or kinked ssDNA by keeping the native global structure of the trimerization core largely intact. The fluorescence data fit nicely with this model featured with a full engagement of W528 in contact with the 16^{th} nt and W107 with 24^{th} nt via aromatic base stacking. Also interestingly, in the domain structure of DBD-C (24), W528 is located just outside the exit and below the palm surface of the binding cleft of DBD-C with its aromatic rings facing up to the ssDNA binding path. Our proposed structure indicates that maximization of the interaction of this residue with the 16^{th} nt of substrate facilitates the ssDNA bending, implying that W528 may play an important role in ssDNA bending. It should be pointed out, however, that there are obvious limitations for this model which was generated with many assumptions. First, the model involves only the four major DBDs without consideration of whether DBD-AB interacts with DBD-CD. Domains F and E, as well as the C-terminal domain and the non-domain N-terminus of RPA32, are not included. Second, the structure of the trimerization core was assumed to be globally unchanged upon ssDNA binding so that the corresponding structure of the model is comparable to the crystallographic structure

of the core (24). Third, an average length of 4.8 Å per nucleotide of the ssDNA was applied throughout the modeling. Fourth, no change was assumed to the DBDs-AB-8nt ssDNA complex structure as previously reported (33). Finally, it should be mentioned that the docked ssDNA fragment between DBD-B and C could also be curved due to the flexibility of the 18-amino acids linker, although in our modeling it was kept straight. In addition, because of such a long linker, the relative spatial positioning between DBD-B and DBD-C of native RPA in solution is likely to be dynamic in the absence of ssDNA.

In conclusion, the present study provided some important structural details on human RPA-ssDNA complex formation at single nucleotide resolution using ssDNA as a molecular ruler. As summarized in Figure 5B, our studysuggests that the W528 and W107 residues of RPA are in direct contact with the 16^{th} and 24^{th} nt of ssDNA numbered from the 5′-end, respectively. Using the co-crystal structure of DBD-AB-ssDNA complex (33) as a model, the average length per nucleotide in binding was estimated to be 4.8 A/nt, which is also consistent with a previous determination (41). With this information combined with our results, we propose that DBD-B and DBD-C are spaced by about 4 nt via a long flexible and unstructured peptide loop, while DBD-C and DBD-D are separated by approximately 7 nt. Our results also suggest that the four DBDs occlude about 26 nucleotides of ssDNA (Figure 5B). However, we speculate that a few more nucleotides may be also needed to facilitate the ssDNA binding of DBD-D, implying that other parts or domains of RPA could also be partially or indirectly involved so that 30 nucleotides of ssDNA are occluded by RPA.

Acknowledgements

We thank Dr. Phillip Musich for critical reading of the manuscript. This study was supported by National Institutes of Health grant CA86927 (to Y.Z.).

References

1. Zou Y, Liu Y, Wu X, Shell SM. Functions of human replication protein A (RPA): from DNA replication to DNA damage and stress responses. J Cell Physiol 2006;208:267–273. [PubMed: 16523492]
2. Liu Y, Yang Z, Utzat CD, Liu Y, Geacintov NE, Basu AK, Zou Y. Interactions of human replication protein A with single-stranded DNA adducts. Biochem J 2005;385:519–526. [PubMed: 15362978]
3. Binz SK, Sheehan AM, Wold MS. Replication protein A phosphorylation and the cellular response to DNA damage. DNA Repair (Amst) 2004;3:1015–1024. [PubMed: 15279788]
4. Iftode C, Daniely Y, Borowiec JA. Replication protein A (RPA): the eukaryotic SSB. Crit Rev Biochem Mol Biol 1999;34:141–180. [PubMed: 10473346]
5. He Z, Henricksen LA, Wold MS, Ingles CJ. RPA involvement in the damage-recognition and incision steps of nucleotide excision repair. Nature 1995;374:566–569. [PubMed: 7700386]
6. Sancar A, Lindsey-Boltz LA, Unsal-Kacmaz K, Linn S. Molecular mechanisms of mammalian DNA repair and the DNA damage checkpoints. Annu Rev Biochem 2004;73:39–85. [PubMed: 15189136]
7. Wold MS. Replication protein A: a heterotrimeric, single-stranded DNA-binding protein required for eukaryotic DNA metabolism. Annu Rev Biochem 1997;66:61–92. [PubMed: 9242902]
8. Wu X, Shell SM, Zou Y. Interaction and colocalization of Rad9/Rad1/Hus1 checkpoint complex with replication protein A in human cells. Oncogene 2005;24:4728–4735. [PubMed: 15897895]
9. Zou L, Elledge SJ. Sensing DNA damage through ATRIP recognition of RPA-ssDNA complexes. Science 2003;300:1542–1548. [PubMed: 12791985]
10. Zou L, Liu D, Elledge SJ. Replication protein A-mediated recruitment and activation of Rad17 complexes. Proc Natl Acad Sci U S A 2003;100:13827–13832. [PubMed: 14605214]
11. Liu VF, Weaver DT. The ionizing radiation-induced replication protein A phosphorylation response differs between ataxia telangiectasia and normal human cells. Mol Cell Biol 1993;13:7222–7231. [PubMed: 8246944]

12. Wu X, Yang Z, Liu Y, Zou Y. Preferential localization of hyperphosphorylated replication protein A to double strand break repair and checkpoint complexes upon DNA damage. Biochem J 2005;391:473–480. [PubMed: 15929725]
13. Liu Y, Liu Y, Yang Z, Utzat C, Wang G, Basu AK, Zou Y. Cooperative interaction of human XPA stabilizes and enhances specific binding of XPA to DNA damage. Biochemistry 2005;44:7361–7368. [PubMed: 15882075]
14. Vassin VM, Wold MS, Borowiec JA. Replication protein A (RPA) phosphorylation prevents RPA association with replication centers. Mol Cell Biol 2004;24:1930–1943. [PubMed: 14966274]
15. Nuss JE, Patrick SM, Oakley GG, Alter GM, Robison JG, Dixon K, Turchi JJ. DNA damage induced hyperphosphorylation of replication protein A. 1. Identification of novel sites of phosphorylation in response to DNA damage. Biochemistry 2005;44:8428–8437. [PubMed: 15938632]
16. Patrick SM, Oakley GG, Dixon K, Turchi JJ. DNA damage induced hyperphosphorylation of replication protein A. 2. Characterization of DNA binding activity, protein interactions, and activity in DNA replication and repair. Biochemistry 2005;44:8438–8448. [PubMed: 15938633]
17. Liu Y, Kvaratskhelia M, Hess S, Qu Y, Zou Y. Modulation of Replication Protein A Function by Its Hyperphosphorylation-induced Conformational Change Involving DNA Binding Domain *B*. J Biol Chem 2005;280:32775–32783. [PubMed: 16006651]
18. Olson E, Nievera CJ, Klimovich V, Fanning E, Wu X. RPA2 is a direct downstream target for ATR to regulate the S-phase checkpoint. J Biol Chem. 2006
19. Fanning E, Klimovich V, Nager AR. A dynamic model for replication protein A (RPA) function in DNA processing pathways. Nucleic Acids Res 2006;34:4126–4137. [PubMed: 16935876]
20. Kim C, Wold MS. Recombinant human replication protein A binds to polynucleotides with low cooperativity. Biochemistry 1995;34:2058–2064. [PubMed: 7849064]
21. Kim C, Paulus BF, Wold MS. Interactions of human replication protein A with oligonucleotides. Biochemistry 1994;33:14197–14206. [PubMed: 7947831]
22. Kim C, Snyder RO, Wold MS. Binding properties of replication protein A from human and yeast cells. Mol Cell Biol 1992;12:3050–3059. [PubMed: 1320195]
23. Brill SJ, Bastin-Shanower S. Identification and characterization of the fourth single-stranded-DNA binding domain of replication protein A. Mol Cell Biol 1998;18:7225–7234. [PubMed: 9819409]
24. Bochkareva E, Korolev S, Lees-Miller SP, Bochkarev A. Structure of the RPA trimerization core and its role in the multistep DNA-binding mechanism of RPA. Embo J 2002;21:1855–1863. [PubMed: 11927569]
25. Bastin-Shanower SA, Brill SJ. Functional analysis of the four DNA binding domains of replication protein A. The role of RPA2 in ssDNA binding. J Biol Chem 2001;276:36446–36453. [PubMed: 11479296]
26. de Laat WL, Appeldoorn E, Sugasawa K, Weterings E, Jaspers NG, Hoeijmakers JH. DNA-binding polarity of human replication protein A positions nucleases in nucleotide excision repair. Genes Dev 1998;12:2598–2609. [PubMed: 9716411]
27. Kolpashchikov DM, Weisshart K, Nasheuer HP, Khodyreva SN, Fanning E, Favre A, Lavrik OI. Interaction of the p70 subunit of RPA with a DNA template directs p32 to the 3′-end of nascent DNA. FEBS Lett 1999;450:131–134. [PubMed: 10350071]
28. Iftode C, Borowiec JA. 5′--> 3′ molecular polarity of human replication protein A (hRPA) binding to pseudo-origin DNA substrates. Biochemistry 2000;39:11970–11981. [PubMed: 11009611]
29. Kolpashchikov DM, Khodyreva SN, Khlimankov DY, Wold MS, Favre A, Lavrik OI. Polarity of human replication protein A binding to DNA. Nucleic Acids Res 2001;29:373–379. [PubMed: 11139606]
30. Bochkarev A, Bochkareva E. From RPA to BRCA2: lessons from single-stranded DNA binding by the OB-fold. Curr Opin Struct Biol 2004;14:36–42. [PubMed: 15102447]
31. Blackwell LJ, Borowiec JA. Human replication protein A binds single-stranded DNA in two distinct complexes. Mol Cell Biol 1994;14:3993–4001. [PubMed: 8196638]
32. Bochkareva E, Belegu V, Korolev S, Bochkarev A. Structure of the major single-stranded DNA-binding domain of replication protein A suggests a dynamic mechanism for DNA binding. Embo J 2001;20:612–618. [PubMed: 11157767]

33. Bochkarev A, Pfuetzner RA, Edwards AM, Frappier L. Structure of the single-stranded-DNA-binding domain of replication protein A bound to DNA. Nature 1997;385:176–181. [PubMed: 8990123]
34. Arunkumar AI, Stauffer ME, Bochkareva E, Bochkarev A, Chazin WJ. Independent and coordinated functions of replication protein A tandem high affinity single-stranded DNA binding domains. J Biol Chem 2003;278:41077–41082. [PubMed: 12881520]
35. Daughdrill GW, Ackerman J, Isern NG, Botuyan MV, Arrowsmith C, Wold MS, Lowry DF. The weak interdomain coupling observed in the 70 kDa subunit of human replication protein A is unaffected by ssDNA binding. Nucleic Acids Res 2001;29:3270–3276. [PubMed: 11470885]
36. Lee JH, Park CJ, Arunkumar AI, Chazin WJ, Choi BS. NMR study on the interaction between RPA and DNA decamer containing cis-syn cyclobutane pyrimidine dimer in the presence of XPA: implication for damage verification and strand-specific dual incision in nucleotide excision repair. Nucleic Acids Res 2003;31:4747–4754. [PubMed: 12907715]
37. Bochkarev A, Bochkareva E, Frappier L, Edwards AM. The crystal structure of the complex of replication protein A subunits RPA32 and RPA14 reveals a mechanism for single-stranded DNA binding. Embo J 1999;18:4498–4504. [PubMed: 10449415]
38. Mer G, Bochkarev A, Gupta R, Bochkareva E, Frappier L, Ingles CJ, Edwards AM, Chazin WJ. Structural basis for the recognition of DNA repair proteins UNG2, XPA, and RAD52 by replication factor RPA. Cell 2000;103:449–456. [PubMed: 11081631]
39. Jacobs DM, Lipton AS, Isern NG, Daughdrill GW, Lowry DF, Gomes X, Wold MS. Human replication protein A: global fold of the N-terminal RPA-70 domain reveals a basic cleft and flexible C-terminal linker. J Biomol NMR 1999;14:321–331. [PubMed: 10526407]
40. Lavrik OL, Kolpashchikov DM, Weisshart K, Nasheuer HP, Khodyreva SN, Favre A. RPA subunit arrangement near the 3′-end of the primer is modulated by the length of the template strand and cooperative protein interactions. Nucleic Acids Res 1999;27:4235–4240. [PubMed: 10518616]
41. Treuner K, Ramsperger U, Knippers R. Replication protein A induces the unwinding of long double-stranded DNA regions. J Mol Biol 1996;259:104–112. [PubMed: 8648638]
42. Blackwell LJ, Borowiec JA, Masrangelo IA. Single-stranded-DNA binding alters human replication protein A structure and facilitates interaction with DNA-dependent protein kinase. Mol Cell Biol 1996;16:4798–4807. [PubMed: 8756638]
43. Binz SK, Lao Y, Lowry DF, Wold MS. The phosphorylation domain of the 32-kDa subunit of replication protein A (RPA) modulates RPA-DNA interactions. Evidence for an intersubunit interaction. J Biol Chem 2003;278:35584–35591. [PubMed: 12819197]
44. Shell SM, Hess S, Kvaratskhelia M, Zou Y. Mass spectrometric identification of lysines involved in the interaction of human replication protein A with single-stranded DNA. Biochemistry 2005;44:971–978. [PubMed: 15654753]
45. Yang ZG, Liu Y, Mao LY, Zhang JT, Zou Y. Dimerization of human XPA and formation of XPA2-RPA protein complex. Biochemistry 2002;41:13012–13020. [PubMed: 12390028]
46. Schwieters CD, Kuszewski JJ, Tjandra N, Clore GM. The Xplor-NIH NMR molecular structure determination package. J Magn Reson 2003;160:65–73. [PubMed: 12565051]
47. Lakowicz, JR. Principle of Fluorescence Spectroscopy. 2. 1999.
48. Ma H, Zou Y. Theramodynamic characterization of the interaction of mutant UvrB protein with damaged DNA. Biochemistry 2004;43:4206–4211. [PubMed: 15065864]

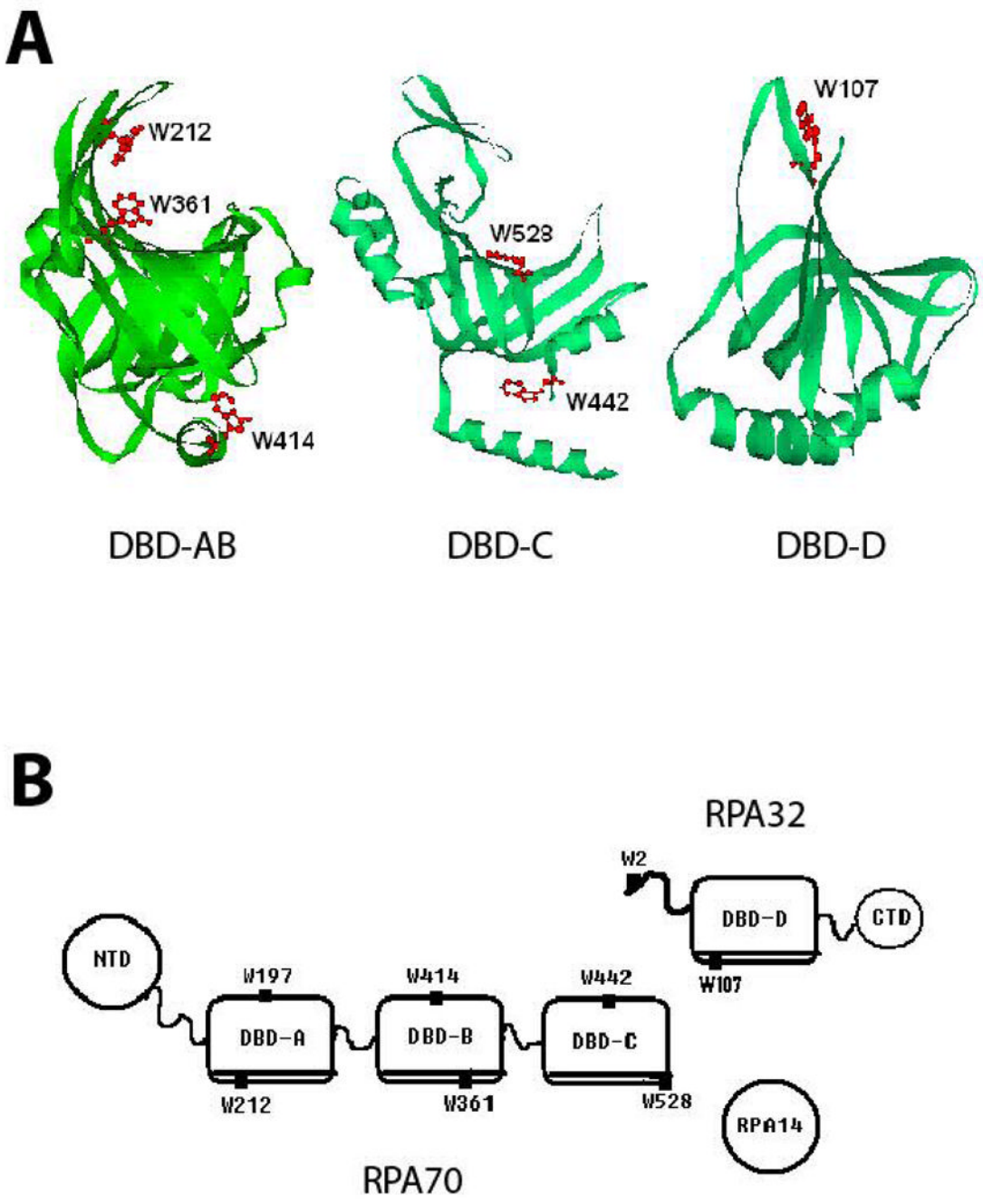

Figure 1.

Structural characters of RPA. Panel A: structures of DBD-AB, DBD-C, and DBD-D (PDB ID: 1jmc and 111o from refs. 31 and 35). The DBDs are positioned by projecting the ssDNA binding cleft in the same direction. The tryptophan residues are marked and colored in red. Panel B: schematic representation of RPA structure. The four DBDs are presented as boxes, the ssDNA binding interfaces are shown in double lines, the loops linking the domains are presented as thin line, and the flexible N-terminus of RPA32 as thick line. NTD stands for the N-terminal domain of RPA70, and CTD for the C-terminal domain of RPA32. The tryptophan residues are marked based on the available domain structures of RPA.

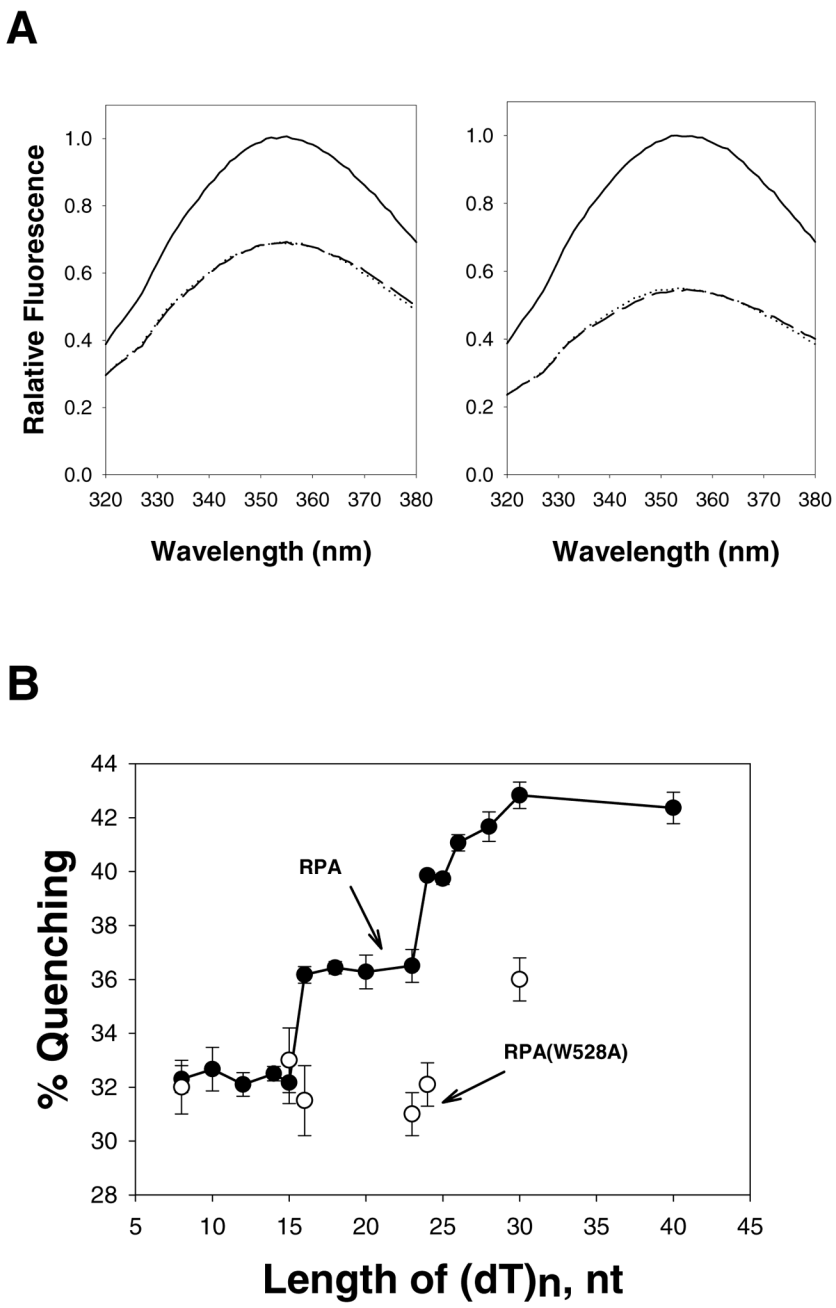

Figure 2.

Dependence of intrinsic tryptophan fluorescence quenching of RPA on its binding to varying lengths of oligonucleotide dT. RPA was subjected to the fluorescence measurements at 25 °C with the excitation wavelength set at 295 nm. Panel A: representative tryptophan fluorescence spectra of RPA (90 nM) in the presence and absence of ssDNA. Solid line, RPA; dotted line, RPA plus 2 μM $(dT)_8$ (left panel) or $(dT)_{30}$ (right panel); and dash line, RPA plus 4 μM $(dT)_n$ with the lengths as indicated. Panel B: quenching of tryptophan fluorescence (353 nm) of native RPA upon binding to ssDNA of increasing lengths (filled circle). The % quenching is defined in the Experimental Procedures, and the error bars represent the standard deviation

from at least three independent measurements. The open circles represent the same binding of RPA(W528A) mutant to ssDNA.

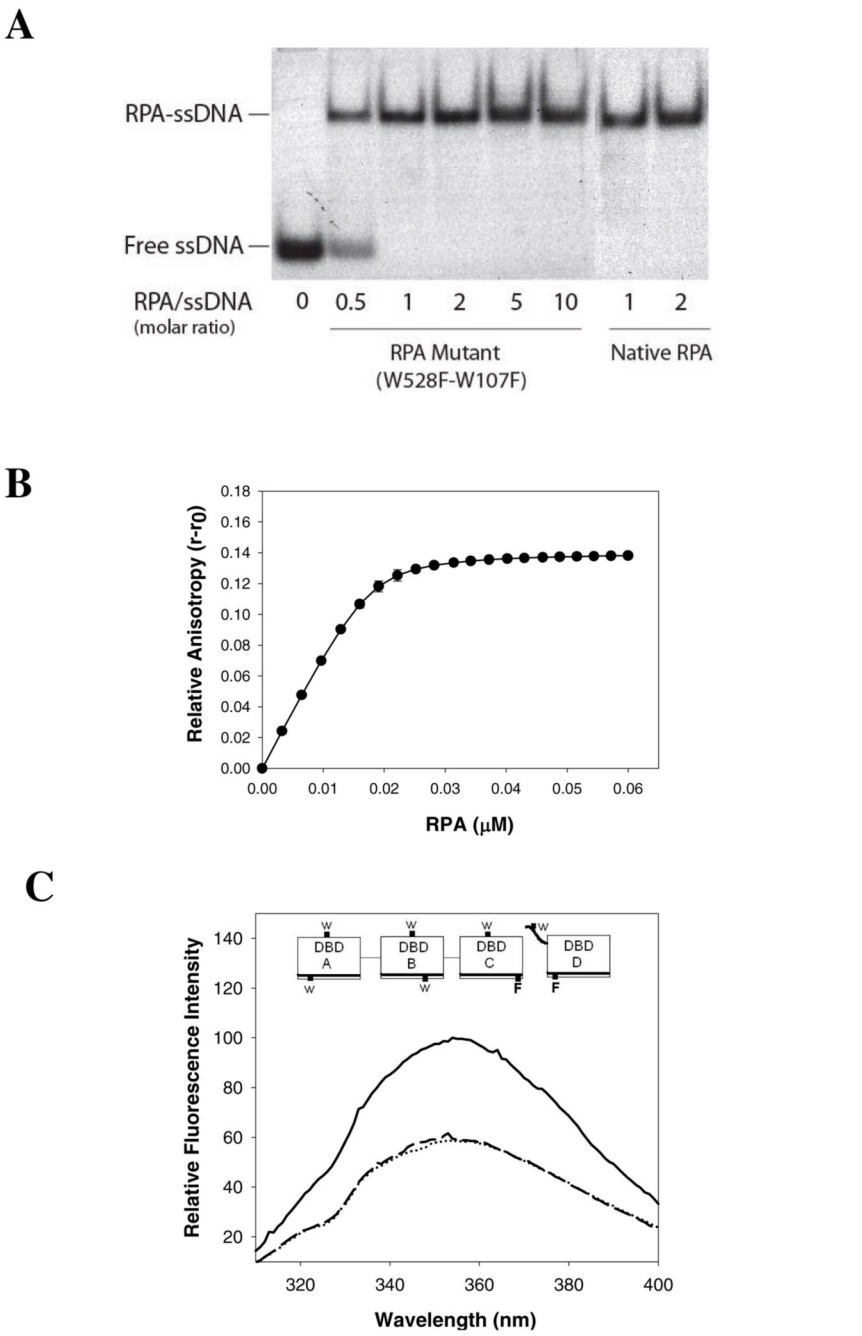

Figure 3.

Interactions of RPA mutant with ssDNA. Panel A: binding of the native RPA and the RPA mutant protein with two point mutations of W528F of DBD-C and W107F of DBD-D to $(dT)_{30}$ ssDNA (4 nM) as analyzed by gel mobility shift assays. Panel B: Titration of the RPA mutant interaction with $(dT)_{30}$ measured by fluorescence anisotropy. The binding isotherms were fitted by non-linear least square method as described previously (2,48). Panel C: the RPA mutant was subjected to fluorescence measurements (λ_{ex} = 295 nm) in the presence and absence of saturation concentrations of ssDNA $(dT)_8$ and $(dT)_{30}$. The solid line is for RPA mutant free of ssDNA, dash line for the RPA mutant-dT8mer complex, and dotted line for the RPA mutant-$(dT)_{30}$ complex. The insertion shows the mutation positions in RPA DBDs, where W528 in

the DBD-C of RPA70, and W107 in DBD-D of RPA32 have been substituted with phenylalanine, The W stands for tryptophan residue, and F for phenylalanine residue.

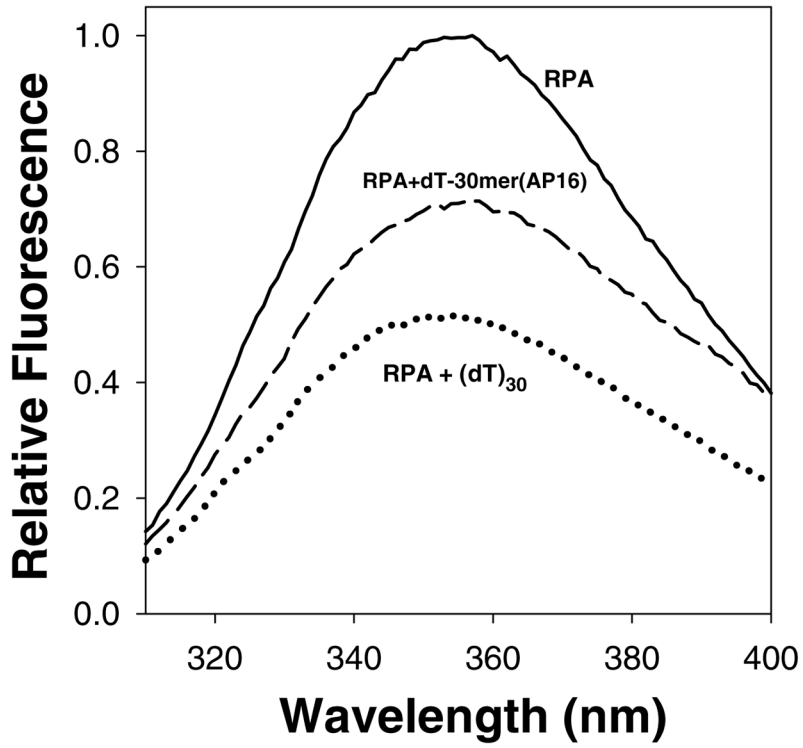

Figure 4.

Fluorescence quenching of RPA upon binding to $(dT)_{30}$ or dT-30mer with an apyrimidinic (AP) site at the 16^{th} nt from 5′-end. RPA (nM) was subjected to the tryptophan fluorescence measurements in the presence or absence of ssDNA substrates (2 μM) at 25 °C with the excitation wavelength set at 295 nm. Solid line, RPA; dotted line, RPA plus 2 μM $(dT)_{30}$; and dash line, RPA plus dT-30mer(AP16).

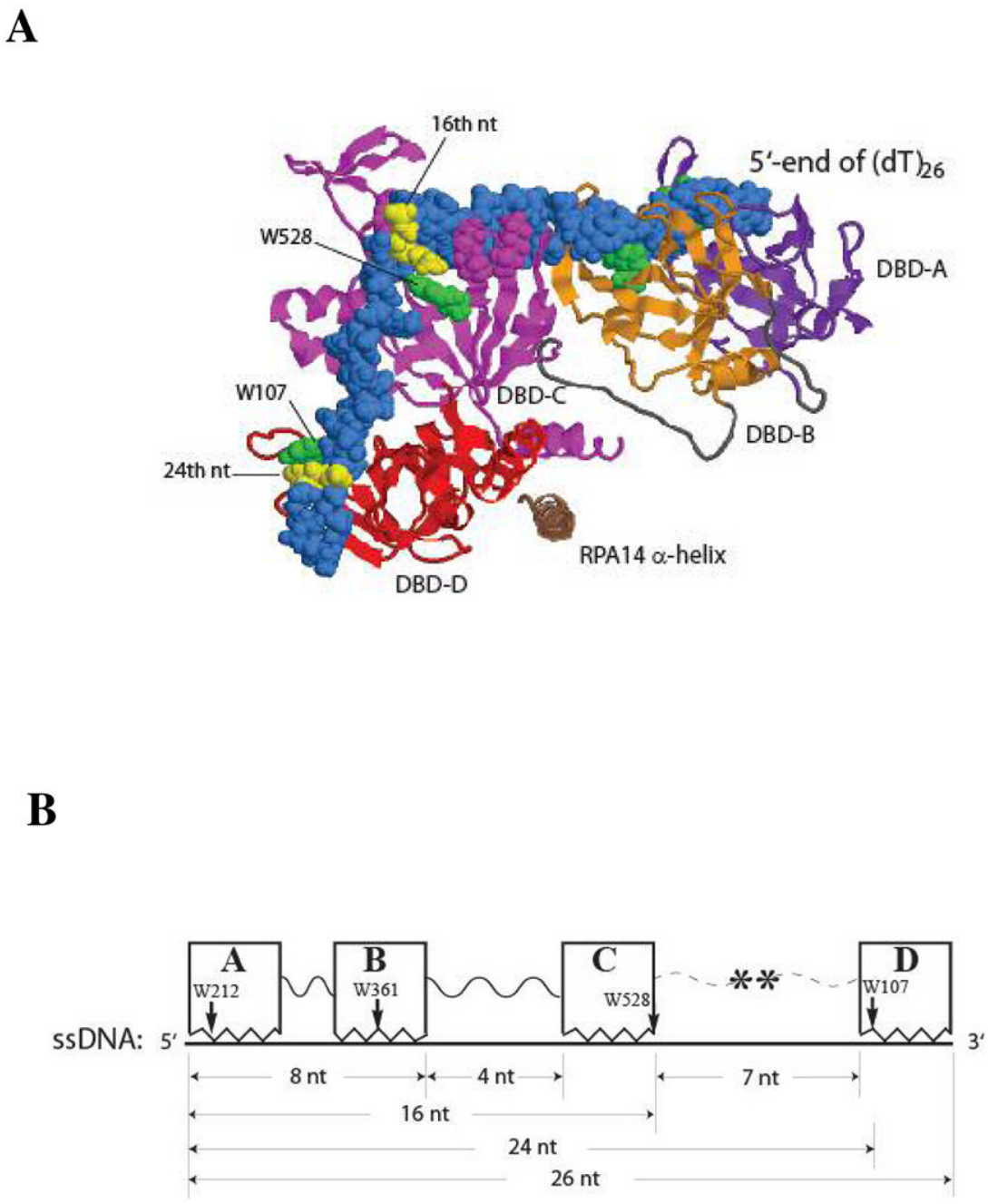

Figure 5.

A structural model of RPA DBDs-ABCD-$(dT)_{26}$ ssDNA complex formation. Panel A: the structures are displayed using RASMOL software (48), and were constructed based on our fluorescence spectroscopic data and the available domain structures of RPA (31,35). The DBD-A, B, C, D domains are colored in purple, orange, magenta, and red, respectively. The α-helix of the RPA14 protein is colored in brown. The loops linking DBD-A and B, DBD-B and C are colored in grey. The ssDNA is colored in blue and displayed in space-filling format, with dT16 and dT24 in yellow. The four Trp residues that are presumed to interact with DNA are colored in green. Panel B: schematic representation of the dimension of RPA-ssDNA complex. The boxes A, B, C, and D represent DBD-A, DBD-B, DBD-C, and DBD-D of RPA, respectively.

Both DBD-C and DBD-D have a ssDNA binding cleft of about 3 nt long, as derived from the domain structural data of RPA (31,35). The ssDNA is plotted in thick line. The arrows indicate the relative positions of the tryptophan residues of individual DBDs in binding.

Table 1

Dissociation constants for native RPA and RPA(W528A) mutant binding to the 5′-fluorecein labeled $(dT)_{30}$

RPA	$K_{d,obs}$ (nM)
Native	3.1 ±0.6
W528A	8.2 ±0.5